

## Atomic-Level Understanding of “Asymmetric Twins” in Boron Carbide

Kelvin Y. Xie,<sup>1</sup> Qi An,<sup>2</sup> M. Fatih Toksoy,<sup>3</sup> James W. McCauley,<sup>1,4</sup> Richard A. Haber,<sup>3</sup>  
William A. Goddard III,<sup>2</sup> and Kevin J. Hemker<sup>1,\*</sup>

<sup>1</sup>Department of Mechanical Engineering, Johns Hopkins University, Baltimore, Maryland 21218, USA

<sup>2</sup>Materials and Process Simulation Center, California Institute of Technology, Pasadena, California 91125, USA

<sup>3</sup>Ceramic and Composite Materials Center, Rutgers University, New Brunswick, New Jersey 08854, USA

<sup>4</sup>U.S. Army Research Lab, Aberdeen Proving Ground, Maryland 21005, USA

(Received 8 July 2015; published 20 October 2015)

Recent observations of planar defects in boron carbide have been shown to deviate from perfect mirror symmetry and are referred to as “asymmetric twins.” Here, we demonstrate that these asymmetric twins are really phase boundaries that form in stoichiometric  $B_4C$  (i.e.,  $B_{12}C_3$ ) but not in  $B_{13}C_2$ . TEM observations and *ab initio* simulations have been coupled to show that these planar defects result from an interplay of stoichiometry, atomic positioning, icosahedral twinning, and structural hierarchy. The composition of icosahedra in  $B_4C$  is  $B_{11}C$  and translation of the carbon atom from a polar to equatorial site leads to a shift in bonding and a slight distortion of the lattice. No such distortion is observed in boron-rich  $B_{13}C_2$  because the icosahedra do not contain carbon. Implications for tailoring boron carbide with stoichiometry and extrapolations to other hierarchical crystalline materials are discussed.

DOI: 10.1103/PhysRevLett.115.175501

PACS numbers: 61.72.Nn, 61.50.Ah, 61.50.Nw

In crystalline materials the formation of twin boundaries, which separate adjacent crystallographic regions whose lattices are related by mirror symmetry, have been associated with both crystal growth and deformation processes. Because of their inherent symmetry, twin boundaries are usually coherent, have low interfacial energy, and are relatively stable as compared to general grain boundaries of random misorientation [1]. The formation of twins and the presence of twin boundaries can significantly affect the plasticity and strength of materials. The latter is demonstrated by the development of twinning-induced steels [2], recent observations that nanotwinned Cu is ten times stronger than coarse-grained Cu [3], and by reports that nanotwinned cubic BN is harder than diamond [4,5]. In this light, understanding how twins are formed and developing effective strategies for incorporating twin boundaries into polycrystalline microstructures offer an attractive approach for enhancing the mechanical response of metals and ceramics.

Twin boundaries in relatively simple systems, such as fcc, bcc, and hcp, can be easily identified with the unambiguous twin planes and misorientation angles. However, as the crystal structure becomes more complicated and exhibits secondary and tertiary structural hierarchy (e.g., boron carbide [6]), the matrix-twin relationship can be complex. Recently, Fujita *et al.* discovered a new type of planar defect in boron carbide and characterized it with spherical-aberration-corrected scanning transmission electron microscopy (STEM) [7]. At first glance their high-resolution STEM images suggest that the planar defects are conventional twin boundaries, but closer investigation reveals that the lattices do not mirror each other exactly,

the angle between the (100) and (010) planes differs by  $\sim 2^\circ$  on either side of the boundary. Upon realizing the loss of mirror symmetry, the authors named these planar defects “asymmetric twins” and stated that their formation mechanisms were not fully understood. At this point, it is important to note that Fujita’s lattice images show the geometric arrangement of the icosahedra, but do not give direct atomic positions because even spherical aberration corrected STEM does not have the resolution to image individual boron and carbon atoms within the icosahedra [7,8].

In the present study, TEM observations and *ab initio* simulations are combined to demonstrate that the formation of what Fujita has termed asymmetric twins is related to the underlying stoichiometry of boron carbide, and we explain why. Both asymmetric and symmetric twins were observed in  $B_4C$  (i.e.,  $B_{12}C_3$ ) but only symmetric twins in  $B_{13}C_2$ . Our combined approach provides convincing evidence that the loss of symmetry is associated with local arrangements of boron and carbon atoms and the bonding that results. The formation of asymmetric twins is directly related to the hierarchical levels of structure that boron carbide possesses, and it is reasonable to assume that such defects may also be present in other crystalline materials with similar levels of complexity.

To investigate the characteristics of asymmetric twins, two boron carbide samples with different stoichiometries ( $B_{12}C_3$  and  $B_{13}C_2$ ) were fabricated. The  $B_{12}C_3$  (i.e.,  $B_4C$ ) samples were produced at Rutgers University by consolidating  $B_4C$  powders (previously synthesized by a rapid carbothermal reduction method) via spark plasma sintering under 50 MPa for 5 min at nominal temperatures exceeding

1900°C, as described in [9]. The B-rich  $B_{13}C_2$  sample was produced at Ceradyne by hot-pressing H. C. Starck grade C amorphous boron and ESK Tetrabor grade 10  $\mu\text{m}$   $B_4C$  powders at 1900–2200°C and 13.8 MPa for approximately an hour [10]. Both sets of samples were processed at temperatures and under conditions that resulted in fully dense boron carbide. TEM thin foils were prepared by slicing the consolidated materials with a diamond saw and then mechanically polishing on diamond lapping papers using a tripod polisher to create a thin wedge. The specimens were further thinned to electron transparency with ion milling. TEM observations were carried out using a CM300FEG TEM to perform high-resolution (HRTEM) phase contrast imaging. To complement and explain the experimental observations, we performed first-principles simulations with the Vienna *ab initio* simulation package (VASP), with specific emphasis on elucidating the lattice angle differences between the asymmetric and symmetric twin boundaries [11,12].

Both  $B_4C$  and boron-rich  $B_{13}C_2$  consolidated samples were used in this study and observed to contain a high twin density [Figs. 1(a) and 1(b)]. The twin densities were found to be nonuniform in both samples. Some grains contained only a few microtwins, while others contained a high density of nanotwins. In some cases, both microtwins and nanotwins were present within the same grain. The chemical composition of both samples was quantified using electron energy loss spectroscopy [Fig. 1(c)] with special precautions to avoid C contamination issues. The EELS measurements were supported by comparisons with lattice parameter measurements via x-ray diffraction and by Raman spectroscopy.

Closer inspection of more than ten boundaries in each sample revealed that both asymmetric ( $\sim 30\%$ ) and symmetric ( $\sim 70\%$ ) twins are present in the  $B_4C$  sample [Figs. 2(a)–2(d)], whereas only symmetric twins were observed in the  $B_{13}C_2$  sample [Figs. 2(e)–2(f)]. The HRTEM image shown in Fig. 2(a) is a typical example of the asymmetric twins observed in  $B_4C$  along the [001] zone axis. The (100) planes of both crystals are marked with solid red lines. The angles between (100) and (010) were measured to be  $\alpha = 73.8 \pm 0.3^\circ$  in the crystal on the left and  $\alpha' = 72.0 \pm 0.4^\circ$  on the right, indicating that the lattices do not mirror each other exactly ( $\alpha \neq \alpha'$ ). These values are comparable to that reported by Fujita *et al.* [7]. To further elucidate the asymmetric nature, we focused on the boundary of Fig. 2(a) and put red “+” markers on the white dots along (100) and (010) planes on the left crystal [Fig. 2(b)]. Note that the white dots are *not* atoms in HRTEM, rather the distances and angles between the white dots represent those between the icosahedra [7]. We then reflected the markers about the boundary with the (100) planes aligned. Now the markers on the right crystal

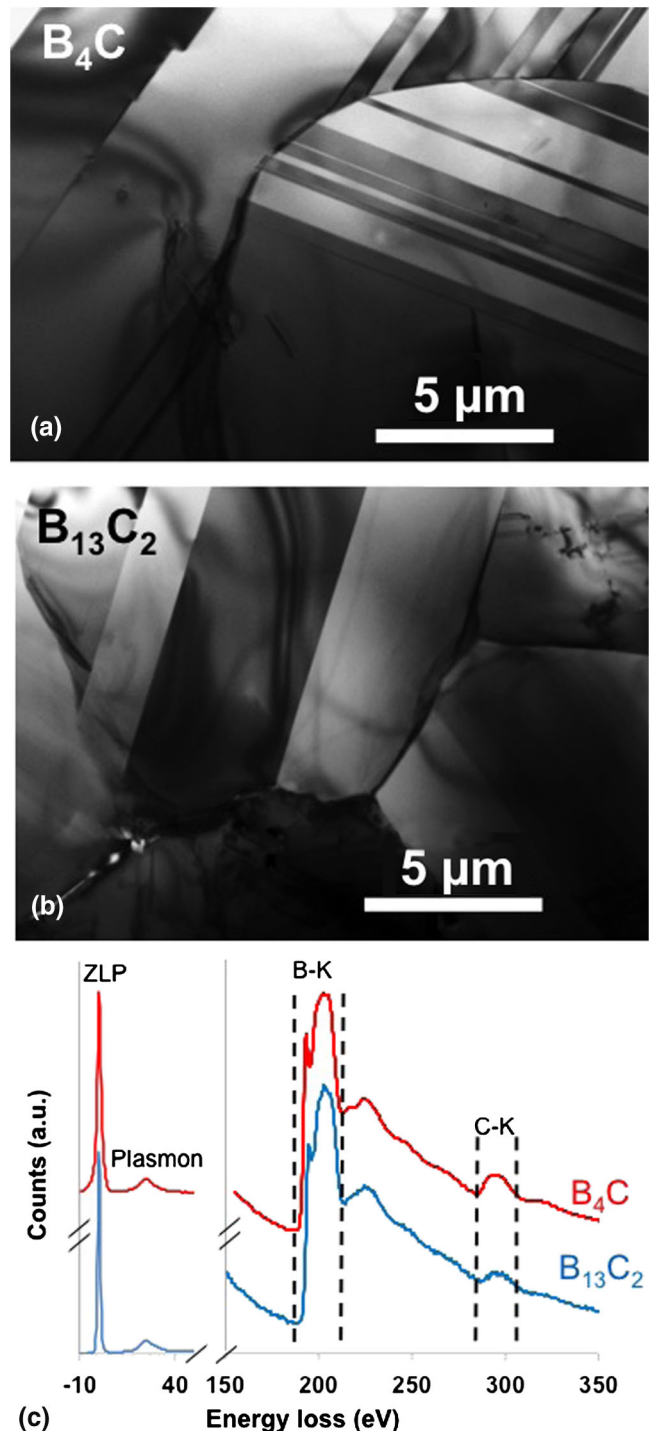


FIG. 1 (color online). Bright-field TEM micrographs of (a)  $B_4C$  and (b)  $B_{13}C_2$ . The diffraction contrast shows that both microtwins and nanotwins are prevalent in both samples. (c) Typical examples of EELS spectra of  $B_4C$  and  $B_{13}C_2$  boron carbide samples. Note the carbon *K*-edge peak in  $B_4C$  is more prominent than  $B_{13}C_2$ . The relative intensities of zero-loss peak (ZLP) and plasmon peak in both examples are very similar, indicating the foil thicknesses, where EELS spectra were acquired, are also similar.

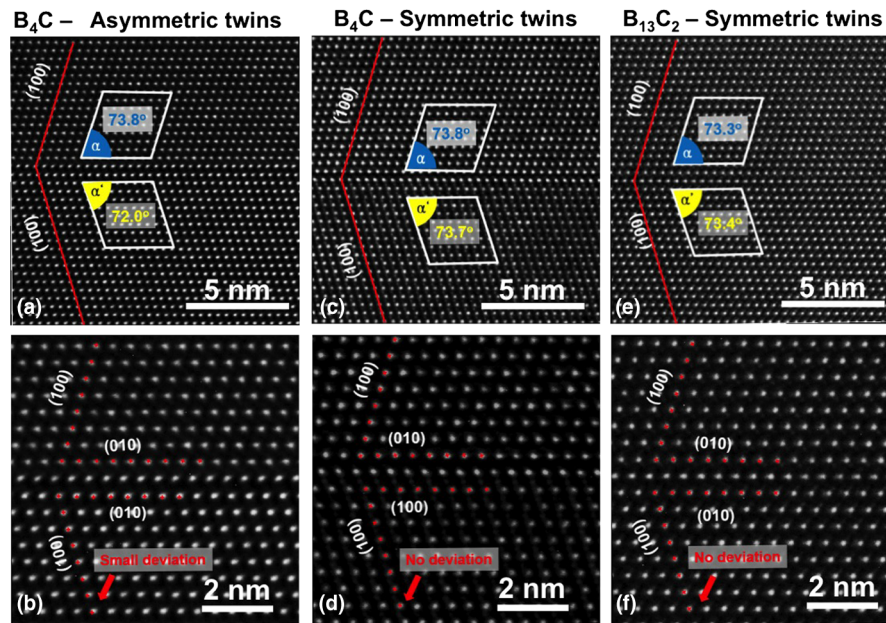


FIG. 2 (color online). HRTEM micrographs showing (a) and (b) an asymmetric twin in  $B_4C$ ; (c) and (d) a symmetric twin in  $B_4C$ ; and (d) and (e) a symmetric twin in  $B_{13}C_2$ . Red solid lines indicate (100) planes in both crystals across the twin boundaries. The “+” are markers labeling the positions of bright spots in the left crystal and then mirrored by the twin boundary to the right crystal to investigate the symmetry across the twin boundaries.

indicate where the bright spots should be if the twin was perfectly symmetric. It can be seen that the markers along the (010) plane in the right crystal do not exactly match the bright spots and a small deviation can be observed. This confirms the fact that the boundary in Figs. 2(a)–2(b) is indeed an “asymmetric twin boundary.” Fujita *et al.* [7] only reported asymmetric twins, but not all of the twin boundaries that we observed in our  $B_4C$  specimens were asymmetric. In many cases, symmetric twins were also observed, as shown in Figs. 2(c)–2(d). The angles in the two crystals associated with this boundary were measured to be  $\alpha = 73.8 \pm 0.3^\circ$  and  $\alpha' = 73.7 \pm 0.3^\circ$ , that  $\alpha = \alpha'$  [Fig. 2(c)]. When the markers on the left grain were reflected to the right, no apparent deviation was observed [Fig. 2(d)]. In the case of B-rich  $B_{13}C_2$ , all ten twin boundaries studied by HRTEM were found to be symmetric with a typical example shown in Figs. 2(e)–2(f). The angles were measured to be  $73.2 \pm 0.2^\circ$  and  $73.3 \pm 0.4^\circ$ , indicating  $\alpha = \alpha'$  [Fig. 2(e)]. The reflected markers also show no apparent deviation [Fig. 2(f)], suggesting it is a symmetric twin boundary.

Understanding the role of stoichiometry on the formation of asymmetric twins requires an understanding of how the atoms are arranged. Experimental HRTEM and STEM images cannot provide this information, but *ab initio* simulations based on density functional theory (DFT) can provide the energies associated with various atomic configurations. In the case of  $B_4C$ , the most stable configuration is  $B_{11}C_p$ -CBC, where the first 12 atoms are contained in the icosahedron, the last 3 atoms make up

the chain, and the subscript  $p$  denotes an atom sitting in a polar site [13–16]. The next stable configuration is  $B_{11}C_e$ -CBC, where  $e$  denotes the carbon occupying the equatorial site. This configuration is 0.54 eV higher than  $B_{11}C_p$ -CBC per unit cell. With the appropriate crystallographic shear translation, the  $B_{11}C_p$ -CBC configuration forms the twin lamella illustrated in Fig. 3(a). Only four complete icosahedra are shown for clarity. The top icosahedron shows the atomic configuration in the matrix, the middle one sits at twin boundary, and the bottom two delineate the twinning process. The twin boundary is marked by a dashed line and the shear translation is indicated by the arrow. Note that the arrow does not lie parallel to the page and has an out-of-plane component. The bottom translucent icosahedron depicts the atomic configuration before shear. The boron atom labeled  $B_1$  is at the equatorial site and is bonded to a carbon atom in a neighboring chain [compare with a matrix icosahedra in Fig. 3(b) for clarity]. The carbon atom in this translucent icosahedron is at the polar site and bonds with a boron atom of the middle icosahedron. After the shear translation to the twin orientation, the bottom icosahedron sits at the new position (the solid one). The  $B_1$  atom is now at the polar site (labeled as  $B_1'$ ), bonding with the middle icosahedron, and the carbon atom in the icosahedron (labeled as  $C'$ ) is at the equatorial site, bonding with the carbon atom in a neighboring chain. In the twin lamella, the atomic configuration changed from the original  $B_{11}C_p$ -CBC to  $B_{11}C_e$ -CBC ( $e$  denotes equatorial site). To verify this hypothesis that different atomic occupancy can change the lattice angles, we constructed the model

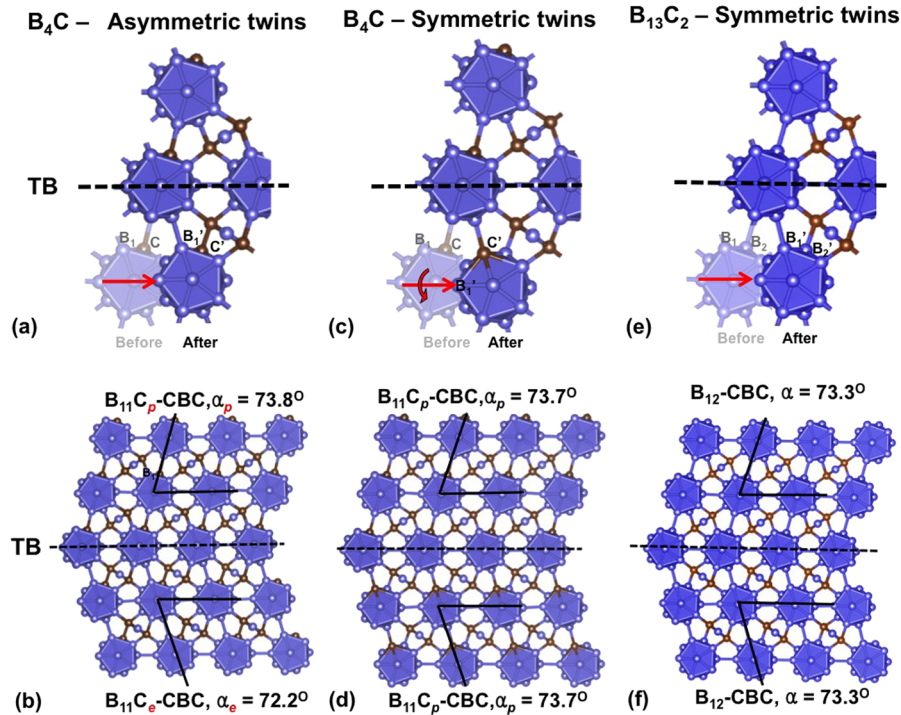


FIG. 3 (color online). (a) An illustration depicting the asymmetric twin formation of  $B_4C$  by shear translation. (b) The relaxed DFT model of the asymmetric twin in  $B_4C$ . (c) An illustration depicting the formation of  $B_4C$  symmetric twins by rotation and shear translation. (d) The relaxed DFT of symmetric twin in  $B_4C$ . (e) An illustration depicting twin formation of  $B_{13}C_2$  by shear translation. (f) The relaxed DFT model.

accordingly and relaxed it using DFT (Perdew-Burke-Ernzerhof flavor) as shown in Fig. 3(b). The angles measured from the simulations are  $73.8^\circ$  for  $B_{11}C_p$ -CBC and  $72.2^\circ$  for  $B_{11}C_e$ -CBC. The slightly smaller angle in  $B_{11}C_e$ -CBC is a result of stronger  $C_{\text{icosaheron}}-C_{\text{chain}}$  interaction that pulled them slightly closer. The angles generated from the simulation agree very well with our experimental measurements of  $73.8^\circ$  and  $72.0^\circ$ , respectively. This suggests that these asymmetric twin boundaries are actually phase boundaries between two very similar phases of  $B_{11}C_p$ -CBC and  $B_{11}C_e$ -CBC.

In addition to these phase boundaries, many symmetric twins were also observed in  $B_4C$  stoichiometry boron carbide. Our DFT calculations indicate that the interfacial energy of the symmetric twin is  $83.2 \text{ mJ/m}^2$  while the interface energy for the asymmetric twin is  $189.2 \text{ mJ/m}^2$ , suggesting that the formation of symmetric  $B_{11}C_p$ -CBC twins is more thermodynamically favorable. Nevertheless, the formation of metastable structures like twins is governed by both kinetics and thermodynamics. Crystallographic translation and rotation of the icosahedra can be used to geometrically transform the matrix into a symmetric twin, as shown in Fig. 3, but it is currently not clear whether the twins form during solid state processing or are the result of thermal or mechanical stresses. Our DFT simulations do suggest that the carbon atom in the bottom translucent icosahedra initially sits at the polar site [Fig. 3(c)]. After rotating to

the boron site labeled  $B_1$  and translating to the twin orientation, now the carbon atom ( $C'$  in the solid bottom icosahedron) still occupies the polar site, but is bonded to a different boron atom from the middle icosahedron. Thus, this combination of crystallographic rotation and translation retains the  $B_{11}C_p$ -CBC atomic configuration in the twinned region, leading to symmetric twin boundaries [Fig. 3(d)].

In the case of  $B_{13}C_2$ , the most stable configuration is  $B_{12}$ -CBC, where the icosahedron is composed of 12 boron atoms, and the shear of the icosahedra does not result in a phase transformation. In the model illustrated in Fig. 3(e), the crystallographic shear translation of the bottom icosahedra changes the bonding: one originally equatorial boron atom ( $B_1$ ) becomes the polar site atom and an originally polar site boron atom becomes an equatorial atom bonding with a chain carbon atom. But the switching in bonding does not change the atomic occupancy in the twinned region; boron still occupies the polar site and the crystal on one side mirrors the other, forming a symmetric twin boundary [Fig. 3(f)]. This careful accounting of atomic positions explains why shear-transformed phase boundaries can form in  $B_4C$  but not in B-rich  $B_{13}C_2$ .

This atomic-level description of the shear-induced phase boundary indicates that stoichiometry and alloying additions can be used to tailor the type and density of planar defects, and thus the attendant mechanical, ballistic, and electrical properties of boron carbide and other boron-based

compounds. Phase diagrams report a wide range of solubility for boron carbide [6], and this solubility may be accommodated by the presence of planar defects, much like Wadsley defects and polysomatic series have been used to describe the modular aspects of minerals [17]. The role of these planar defects is still under debate, but identification of local atomic arrangements at planar boundaries, like the work reported here, is very much needed to elucidate their influence on the overall composition and properties of boron carbide.

In a larger context, our finding that hierarchically structured materials possess a complex array of crystalline defects should be applicable to broad families of ceramics and minerals. The current study identified two necessary criteria for the formation of shear-induced phase boundaries. First, the material must have a hierarchical crystal structure. In boron carbide, the primary structures are 12-atom icosahedra and 3-atom chains, and the secondary structures are rhombohedral unit cells composed of icosahedra and CBC chains. Small changes in the atomic arrangement of the primary building blocks can be reflected as phase boundaries in the secondary structure. Nonhierarchical materials such as, Cu, Mo, Mg, etc., cannot form these phase boundaries because the basic building blocks for the crystals are individual atoms. Second, the primary structure must be polar. The icosahedra in  $B_4C$  are  $B_{11}C$  and a modification in the bonding characteristics of carbon changed the secondary structure. On the other hand,  $B_{12}$  icosahedra in  $B_{13}C_2$  are nonpolar, and do not lead to the formation of the phase boundaries. Therefore, any crystalline material that satisfies the aforementioned two criteria should contain these planar defects. Prospects for an expanded classification of criteria and defect structures seem highly plausible with the integration of ever more sophisticated experimental and computational capabilities.

In summary, our TEM observations and *ab initio* simulations show that asymmetric twins are actually shear-induced phase boundaries that form in  $B_4C$  but not in boron-rich  $B_{13}C_2$ . This novel planar defect results from the interplay of stoichiometry, atomic positioning, twinning, and structural hierarchy. The presence of these planar boundaries and local changes in atomic bonding and structure are expected to influence the mechanical, electrical, and magnetic properties of boron carbide [18–22], and the importance of stoichiometry offers a unique handle for tailoring these properties.

This research was sponsored by the Army Research Laboratory and was accomplished under Cooperative Agreement No. W911NF-12-2-0022. In addition, Q. A. and W. A. G. also received support from the Defense Advanced Research Projects Agency (W31P4Q-13-1-0010, program manager, Judah Goldwasser), and the

National Science Foundation (DMR-1436985). The views and conclusions contained in this document are those of the authors and should not be interpreted as representing the official policies, either expressed or implied, of the Army Research Laboratory or the U.S. Government. “The U.S. Government retains and the publisher, by accepting the paper for publication, acknowledges that the U.S. Government retains a nonexclusive, paid-up, irrevocable, world-wide license to publish or reproduce the published form of this manuscript, or allow others to do so, for U.S. Government purposes.”

---

\*Corresponding author.  
hemker@jhu.edu

- [1] J. W. Christian and S. Mahajan, *Prog. Mater. Sci.* **39**, 1 (1995).
- [2] O. Grässel, L. Krüger, G. Frommeyer, and L. Meyer, *Int. J. Plast.* **16**, 1391 (2000).
- [3] L. Lu, X. Chen, X. Huang, and K. Lu, *Science* **323**, 607 (2009).
- [4] Y. Tian *et al.*, *Nature (London)* **493**, 385 (2013).
- [5] B. Li, H. Sun, and C. Chen, *Nat. Commun.* **5**, 4965 (2014).
- [6] V. Domnich, S. Reynaud, R. A. Haber, and M. Chhowalla, *J. Am. Ceram. Soc.* **94**, 3605 (2011).
- [7] T. Fujita, P. Guan, K. M. Reddy, A. Hirata, J. Guo, and M. Chen, *Appl. Phys. Lett.* **104**, 021907 (2014).
- [8] K. M. Reddy, P. Liu, A. Hirata, T. Fujita, and M. Chen, *Nat. Commun.* **4**, 2483 (2013).
- [9] F. Toksoy, W. Rafaniello, K. Y. Xie, K. J. Hemker, and R. A. Haber (to be published).
- [10] M. Chheda and J. Shih, Army Research Lab internal Report No. CER-231, 2008.
- [11] G. Kresse and J. Hafner, *Phys. Rev. B* **47**, 558 (1993).
- [12] G. Kresse and J. Furthmüller, *Phys. Rev. B* **54**, 11169 (1996).
- [13] R. Lazzari, N. Vast, J. M. Besson, S. Baroni, and A. Dal Corso, *Phys. Rev. Lett.* **83**, 3230 (1999).
- [14] H. Clark and J. Hoard, *J. Am. Chem. Soc.* **65**, 2115 (1943).
- [15] F. Mauri, N. Vast, and C. J. Pickard, *Phys. Rev. Lett.* **87**, 085506 (2001).
- [16] Q. An, W. A. Goddard III, and T. Cheng, *Phys. Rev. Lett.* **113**, 095501 (2014).
- [17] S. Merlino, *Modular Aspects of Minerals* (Eötvös University Press, Budapest, Hungary, 1997), Vol. 1.
- [18] L. Lu, Y. Shen, X. Chen, L. Qian, and K. Lu, *Science* **304**, 422 (2004).
- [19] M. Chen, J. W. McCauley, and K. J. Hemker, *Science* **299**, 1563 (2003).
- [20] G. Fanchini, J. W. McCauley, and M. Chhowalla, *Phys. Rev. Lett.* **97**, 035502 (2006).
- [21] X. Q. Yan, Z. Tang, L. Zhang, J. J. Guo, C. Q. Jin, Y. Zhang, T. Goto, J. W. McCauley, and M. W. Chen, *Phys. Rev. Lett.* **102**, 075505 (2009).
- [22] Q. An and W. A. Goddard III, *Phys. Rev. Lett.* **115**, 105501 (2015).